Versatile and Efficient Targeting Using a Single Nanoparticulate Platform: Application to Cancer and Alzheimer's Disease

Benjamin Le Droumaguet,[†] Julien Nicolas,[†,*] Davide Brambilla,[†] Simona Mura,[†] Andrei Maksimenko,[†] Line De Kimpe,[‡] Elisa Salvati,[§] Cristiano Zona,[⊥] Cristina Airoldi,[⊥] Mara Canovi,[¶] Marco Gobbi,[¶] Magali Noiray,[†] Barbara La Ferla,[⊥] Francesco Nicotra,[⊥] Wiep Scheper,[‡] Orfeu Flores,[#] Massimo Masserini,[§] Karine Andrieux,[†] and Patrick Couvreur[†]

[†]Laboratoire de Physico-Chimie, Pharmacotechnie et Biopharmacie, University Paris-Sud, UMR CNRS 8612, Faculté de Pharmacie, 5 rue Jean-Baptiste Clément, F-92296 Châtenay-Malabry, France, [‡]Department of Genome Analysis, Academic Medical Center, 1105AZ Amsterdam, The Netherlands, [§]Department of Experimental Medicine, University of Milano-Bicocca, 20052 Monza, Italy, [⊥]Department of Biotechnology and Biosciences, University of Milano-Bicocca, 20126 Milano, Italy, [¶]Istituto di Ricerche Farmacologiche "Mario Negri", 20126 Milano, Italy, and [#]Stab Vida, Madan Parque, Rua dos Inventores, 2825-182, Caparica, Portugal

ABSTRACT A versatile and efficient functionalization strategy for polymeric nanoparticles (NPs) has been reported and successfully applied to PEGylated, biodegradable poly(alkyl cyanoacrylate) (PACA) nanocarriers. The relevance of this platform was demonstrated in both the fields of cancer and Alzheimer's disease (AD). Prepared by copper-catalyzed azide—alkyne cycloaddition (CuAAC) and subsequent self-assembly in aqueous solution of amphiphilic copolymers, the resulting functionalized polymeric NPs exhibited requisite characteristics for drug delivery purposes: (i) a biodegradable core made of poly(alkyl cyanoacrylate), (ii) a hydrophilic poly(ethylene glycol) (PEG) outer shell leading to colloidal stabilization, (iii) fluorescent properties provided by the covalent linkage of a rhodamine B-based dye to the polymer backbone, and (iv) surface functionalization with biologically active ligands that enabled specific targeting. The construction method is very versatile and was illustrated by the coupling of a small library of ligands (*e.g.*, biotin, curcumin derivatives, and antibody), resulting in high affinity toward (i) murine lung carcinoma (M109) and human breast cancer (MCF7) cell lines, even in a coculture environment with healthy cells and (ii) the β-amyloid peptide 1—42 ($A\beta_{1-42}$), believed to be the most representative and toxic species in AD, both under its monomeric and fibrillar forms. In the case of AD, the ligand-functionalized NPs exhibited higher affinity toward $A\beta_{1-42}$ species comparatively to other kinds of colloidal systems and led to significant aggregation inhibition and toxicity rescue of $A\beta_{1-42}$ at low molar ratios.

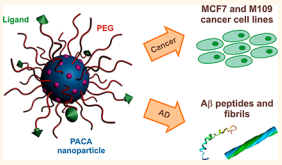

KEYWORDS: nanoparticles · poly(alkyl cyanoacrylate) · Alzheimer's disease · cancer · Aβ peptide · targeting

In the past decade, significant achievements have been witnessed in the field of nanotechnology, especially in material science, electronics, photonics, supramolecular assemblies and drug delivery. In particular, the medical application of nanotechnologies, usually termed nanomedicine,[1−7] has given a crucial impulse to the development of various types of drug-loaded nanocarriers. A great deal of effort is now focused on the engineering of nanoparticulate systems able to serve as efficient diagnostic and/or therapeutic tools against severe diseases, such as cancer or infectious or neurodegenerative disorders.[1,8−19] Among the different classes of materials suitable for drug delivery purposes, nanoparticles (NPs) based on biodegradable polymers have attracted much attention[1,8] due to the flexibility offered by macromolecular synthesis methods, the almost infinite diversity of polymer compositions and their ease of functionalization. However, polymeric nanocarriers designed for drug delivery purposes need to fulfill various criteria that are rarely met in a single colloidal system. Thus, the conception of flexible nanomedicine platforms represents an urgent need in the field. Ideally, they should (i) be biocompatible/biodegradable to allow safe administration; (ii) exhibit stealth properties to escape the immune response; (iii) be functionalized with fluorescent or radioactive probes for traceability/localization purposes and, above all, (iv) display at their periphery suitable ligands in order to achieve the "active targeting" to specific cells or tissues. In addition, the versatility of the envisaged nanoconstructs toward different pathologies, simply by changing the nature of the exposed ligand, may be a highly desirable advantage to engineer a universal nanocarrier.

In this context, biodegradable poly(alkyl cyanoacrylate) (PACA) nanoparticles hold great promise as they have demonstrated

* Address correspondence to julien.nicolas@u-psud.fr.

Received for review January 30, 2012 and accepted June 22, 2012.

Published online June 23, 2012
10.1021/nn3004372

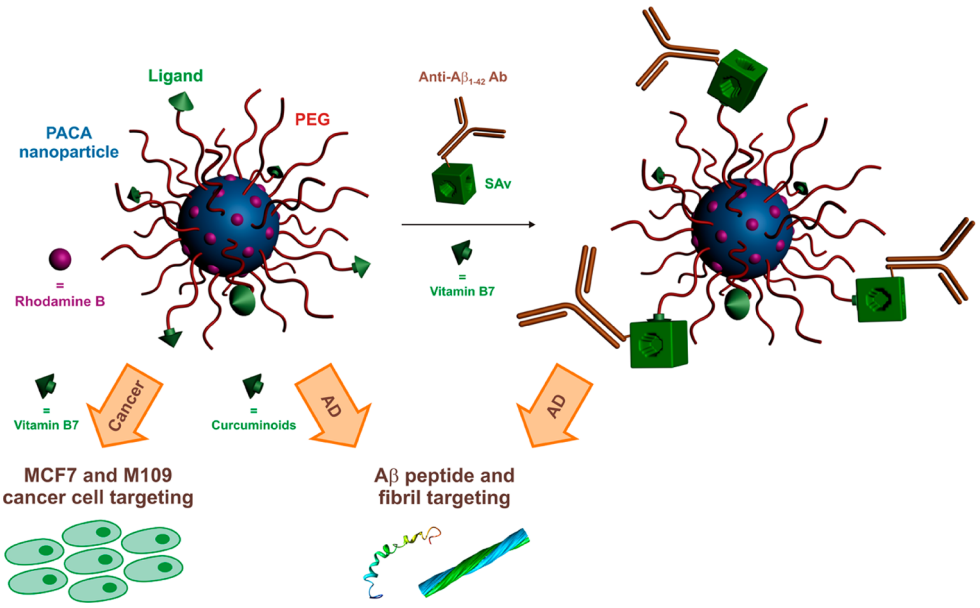

Figure 1. Design of functionalized, PEGylated and biodegradable poly(alkyl cyanoacrylate) (PACA) nanoparticles for specific targeting in the fields of cancer and Alzheimer's disease (AD).

significant preclinical results in multiple pathologies such as cancer[20] and severe infections (viral, bacteriologic, and parasitic)[21] as well as in several metabolic and autoimmune diseases.[22] Currently in phase III clinical trials, doxorubicin-loaded PACA NPs (*i.e.*, Transdrug) have shown improved survival and safety, comparatively to the standard treatment in patients with multidrug resistance (MDR) hepatocarcinoma.[23] Their additional coating with poly(ethylene glycol) (PEG) *via* the use of poly[hexadecyl cyanoacrylate-*co*-methoxypoly(ethylene glycol) cyanoacrylate] (P(HDCA-*co*-MePEGCA)) amphiphilic random copolymer that can self-assemble into well-defined NPs,[24] not only turns them into long-circulating nanocarriers, but also enables them to cross the blood−brain barrier (BBB).[25,26] The latter feature makes them potential drug transporters to the central nervous system (CNS) for the therapy of CNS-related diseases. However, despite these numerous benefits, the functionalization of PACA NPs in order to achieve cell/tissue targeting has been challenging because of the high reactivity of cyanoacrylate monomers and the marked tendency of the resulting polymers to hydrolyse and biodegrade.[27]

Herein is reported the design of a versatile and multifunctional targeted PACA nanoparticulate platform and its successful *in vitro* application in two diseases, namely cancer and Alzheimer's disease (AD), the most common elderly dementia, affecting 35 million people worldwide. While cancer therapy is still an active challenge due to the difficulty of targeting cancer cells, the mechanism involved for AD is still under debate, which hampers any clear and effective therapeutic response. With this in mind, we designed a common colloidal system for which the flexibility of the synthetic strategy allowed ready adaptation of the targeting to the desired pathology simply by choosing the appropriate ligand. In this system, all the required features for drug delivery purposes and cell targeting are gathered: (i) a biodegradable poly(alkyl cyanoacrylate) core,[28] (ii) a PEG outer shell leading to stealth/stabilization features, (iii) fluorescent properties provided by the covalent linkage of a rhodamine B-based dye to the polymer backbone, and (iv) biologically active ligands displayed at their surface for active targeting (Figure 1).

To accomplish specific disease targeting, we developed two original routes. For cancer, whereas folic acid has been extensively employed as cancer cell homing device,[29−31] we used here biotin as a ligand[32] to selectively target different cancer cell lines (*i.e.*, human breast carcinoma MCF7 and murine lung cancer M109) *via* a biotin receptor-mediated uptake, which has scarcely been studied and may open new therapeutic avenues toward cancer therapy. Regarding AD, we functionalized the NPs with either curcumin derivatives, known for their potential role in the prevention and treatment of AD,[29−31] or with a novel specific antibody, *via* the biotin/streptavidin binding strategy, in order to bind not only the β-amyloid peptide 1−42 ($A\beta_{1-42}$) monomer, a biomarker of AD, but also $A\beta_{1-42}$ fibrillar aggregates, usually located in AD brains. Beyond the report of a new methodology for multifunctional NPs construction, this also represents the first example of targeted polymeric NPs for therapeutic application in AD.

RESULTS AND DISCUSSION

Design of a Versatile Nanoparticulate Platform. Multifunctional and biodegradable PACA NPs exhibiting stealth,

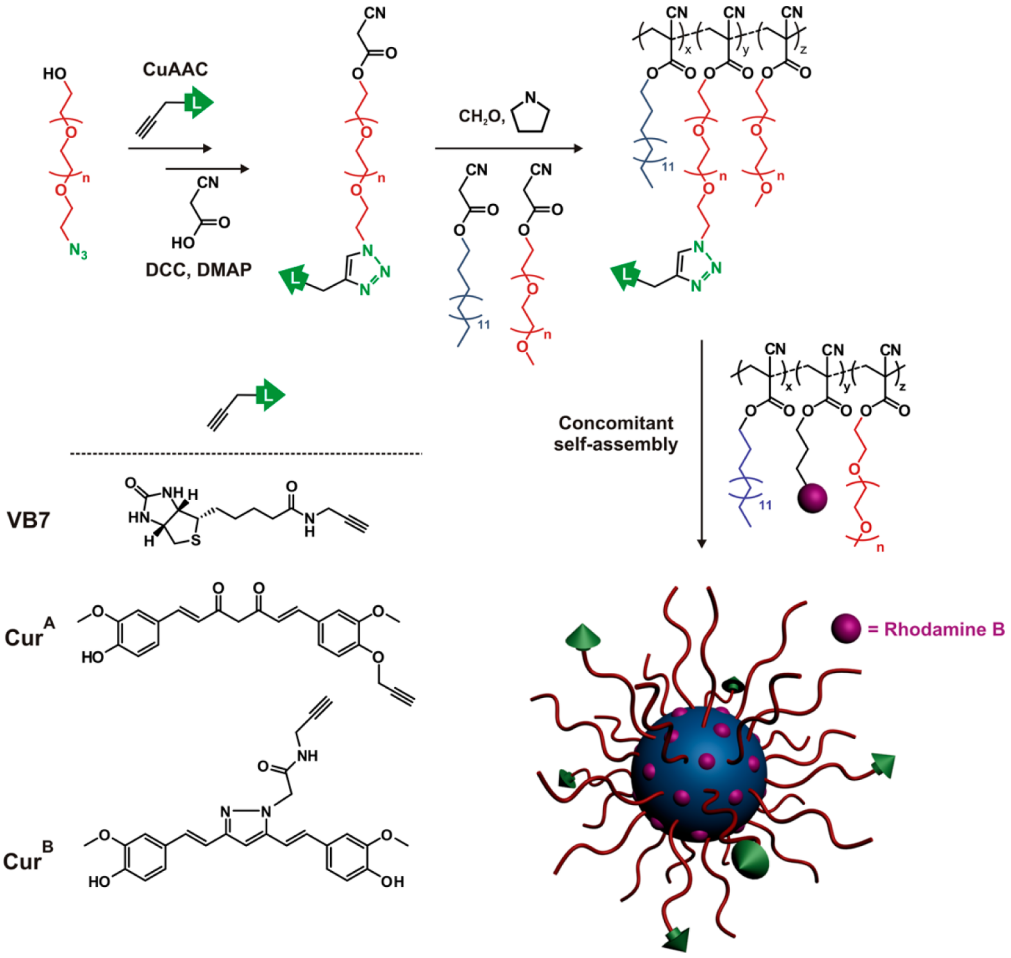

Figure 2. Synthetic pathway to prepare fluorescent, PEGylated and biodegradable poly(alkyl cyanoacrylate) nanoparticles functionalized with biotin (VB7) or curcumin derivatives (Cur^A and Cur^B).

fluorescent, and targeting abilities were synthesized by a combination of (i) copper-catalyzed azide–alkyne cycloaddition (CuAAC)[33] to covalently attach the ligand of interest; (ii) copolymerization of different monomer species to introduce the desired features (fluorescence, targeting moiety, hydrophobicity/hydrophilicity), and (iii) self-assembly in aqueous solution of the resulting amphiphilic copolymers (Figure 2). Practically, a heterobifunctional azidopoly(ethylene glycol) (N_3PEG) was first derivatized with the selected ligand by CuAAC using $CuSO_4$/sodium ascorbate as the catalytic system and turned into its cyanoacetate derivative (Ligand-PEGCA) under DCC-assisted chemistry. This functionalized building block was then terpolymerized with varying amounts of MePEGCA and HDCA by tandem Knoevenagel condensation–Michael addition[24] to afford the corresponding ligand-containing P(MePEGCA-*co*-Ligand-PEGCA-*co*-HDCA) amphiphilic copolymer. Its concomitant self-assembly in aqueous solution with a rhodamine B-tagged P(HDCA-*co*-RCA-*co*-MePEGCA) copolymer[34] allowed the production of the desired colloidal nanocarrier. The versatility of this methodology was illustrated by the synthesis of a small library of biologically active ligands in order to target cancer and Alzheimer's disease.

The use of biotin as a biologically active ligand recently appeared as an elegant way to target cancer cells,[32,35] and represents an original alternative to the extensive use of folic acid toward tumor overexpressed folate receptors. In this view, we prepared PACA NPs functionalized with biotin (**VB7**) *via* the synthesis of a P(HDCA-*co*-**VB7**PEGCA-*co*-MePEGCA) copolymer following the synthetic pathway described in Figure 2. The stoichiometry was chosen so as to achieve a copolymer with 20% of biotinylated PEG chain-ends. A 50/50 P(HDCA-*co*-**VB7**PEGCA-*co*-MePEGCA)/P(HDCA-*co*-RCA-*co*-MePEGCA) copolymer blend was then coself-assembled in aqueous solution to yield a stable suspension of fluorescent NPs exhibiting 10% of biotin at the extremity of the PEG chains (**N1**, Table 1). This amount was selected in order to display a sufficient amount of biotin while not altering stealth/stabilizing properties.

A similar strategy was followed with curcumin derivatives in order to target $A\beta_{1-42}$ peptide and the corresponding fibrils. It has recently been shown that curcumin, a major component of the yellow curry spice turmeric, presents potent antioxidant and

TABLE 1. Compositions and Colloidal Properties of Functionalized and Nonfunctionalized PEGylated Poly(alkyl cyanoacrylate) Nanoparticles

expt.	nanoparticle composition[a]	average diameter (nm)[b]	particle size distribution[b]	ζ-potential (mV)
N0	P(HDCA-*co*-MePEGCA) + P(HDCA-*co*-RCA-*co*-MePEGCA)	106 ± 3.0	0.160	−40.2 ± 10.9
N1	P(HDCA-*co*-**VB7**PEGCA-*co*-MePEGCA) + P(HDCA-*co*-RCA-*co*-MePEGCA)	101 ± 1.8	0.116	−7.9 ± 3.6
N2	P(HDCA-*co*-**Cur^{A}**PEGCA-*co*-MePEGCA) + P(HDCA-*co*-RCA-*co*-MePEGCA)	85 ± 1.6	0.241	−16.2 ± 3.6
N3	P(HDCA-*co*-**Cur^{B}**PEGCA-*co*-MePEGCA) + P(HDCA-*co*-RCA-*co*-MePEGCA)	103 ± 2.8	0.177	−11.7 ± 3.7

[a] Copolymer blends were 50/50 and concentrations of the nanoparticle suspensions were 2.5 mg·mL^{-1} after self-assembly by the nanoprecipitation technique. [b] Determined by dynamic light scattering.

anti-inflammatory activities,[36] but is also able to bind Aβ and to disaggregate Aβ plaques, as well as to prevent fibril and oligomer formation.[37−39] Structure−activity relationships of Aβ-aggregation using curcumin derivatives also revealed that subtle changes in the structure led to severe variations of activity.[40] Therefore, two curcumin derivatives (**Cur^{A}** and **Cur^{B}**) were equipped with an alkyne moiety and employed in the synthetic pathway depicted in Figure 2 to achieve the corresponding curcumin-functionalized NPs (**N2** and **N3**, respectively, Table 1). Whereas the alkyne group was positioned on one aromatic ring for **Cur^{A}**, allowing conformation mobility, the conformation of **Cur^{B}** was blocked *via* the formation of a *N*-heteronuclear pyrazole ring bearing the alkyne moiety. The initial stoichiometry of the reactant was chosen so as to give NPs with 5 mol % of PEG chain functionalized with curcumin.

NPs were characterized by dynamic light scattering (DLS) and transmission electron microscopy (TEM). In all cases, NPs **N0**−**N3** were obtained with average diameters in the 85−106 nm range together with rather narrow particle size distributions (Table 1 and Supporting Information, Figures S1−S4). Long-term stability was also assessed over a period of three days in water and in cell culture medium (endothelial cell basal medium supplemented with fetal bovine serum 5%, hydrocortisone 1.4 μM, basic fibroblast growth factor 1 ng·mL^{-1}, pen-strep 1%, and HEPES 10 mM), the later being a relevant medium since biomedical applications are envisioned (see Supporting Information, Figure S5). ζ-potential measurements for NPs **N1**−**N3** showed negative values from −7.9 to −16.2 mV (Table 1). The presence of ligand at the surface of the NPs only slightly affected the colloidal characteristics but led to a decrease of the absolute surface charge as compared to nonfunctionalized NPs (**N0**), which is a strong indication regarding the effectiveness of the surface modification and the ligand exposure.[41] TEM images, with or without negative staining, revealed spherical-shaped nanoparticle suspensions with average diameters and particle size distributions in good agreement with DLS data (Supporting Information, Figure S6).

Biotin Receptor-Mediated Cancer Cell Targeting. *Targeting of Cancer Cells.* Two cancer cell lines (MCF7 human breast adenocarcinoma cells and M109 murine lung cancer cells), which both overexpress biotin receptors on their surfaces,[32,35] were chosen to evaluate the tumor targeting ability of the biotin-functionalized NPs **N1**. The NPs were added to cells cultured on 6-well plates to target a final nanoparticle concentration of 100 μg·mL^{-1}. It is shown in Figure S7 (Supporting Information) the absence of any cytotoxic effect of both nonfunctionalized (**N0**) and biotinylated (**N1**) NPs for both cell lines at concentrations up to 250 μg·mL^{-1}. After incubation at different time intervals, the cells were collected for analysis of rhodamine B fluorescence by flow cytometry. The internalization of biotinylated NPs **N1** in both cancer cell lines appeared to be about 3-fold higher after 10 h of incubation comparatively to the nonbiotinylated NPs **N0** (Figure 3a and 3b). This result clearly indicated the efficient internalization of targeted NPs in MCF7 and M109 cancer cells.

When cells were incubated with NPs **N1** for 5 h at 4 °C instead of 37 °C, the cell fluorescence intensity dramatically decreased (Figure 3c,d), suggesting that the biotin-functionalized NPs were internalized *via* endocytosis. Moreover, when cells were preincubated with free biotin (2 mM, 1 h) to saturate the biotin receptors on the cancer cell surface before the addition of NPs **N1** (100 μg·mL^{-1}, 37 °C, 5 h), a substantial decrease in fluorescence (by factors of 5 and 8, respectively, for M109 and MCF7 cell lines) was observed (Figure 3c,d), which confirmed a specific receptor-mediated endocytic pathway. Interestingly, when uptake experiments were perfomed with murine leukemia (L1210) cells for which biotin receptors are not overexpressed, it resulted in a poor internalization, thus highlighting the robustness of the targeting pathway (Supporting Information, Figure S10a,b).

The cell uptake and internalization of targeted fluorescent NPs suggested by flow cytometry experiments was confirmed by fluorescence microscopy. As shown in Figure 4, after 5 h incubation, biotinylated NPs **N1** (rhodamine B red staining) significantly accumulated into the MCF7 cell cytoplasm (Ph-FITC green staining) contrary to nonfunctionalized NPs **N0** which barely entered the cells. In addition, the covalent attachment of the rhodamine moiety to the copolymer conducted to a fine fluorescent signal, as opposed to a typical diffuse signal when hydrophobic dyes

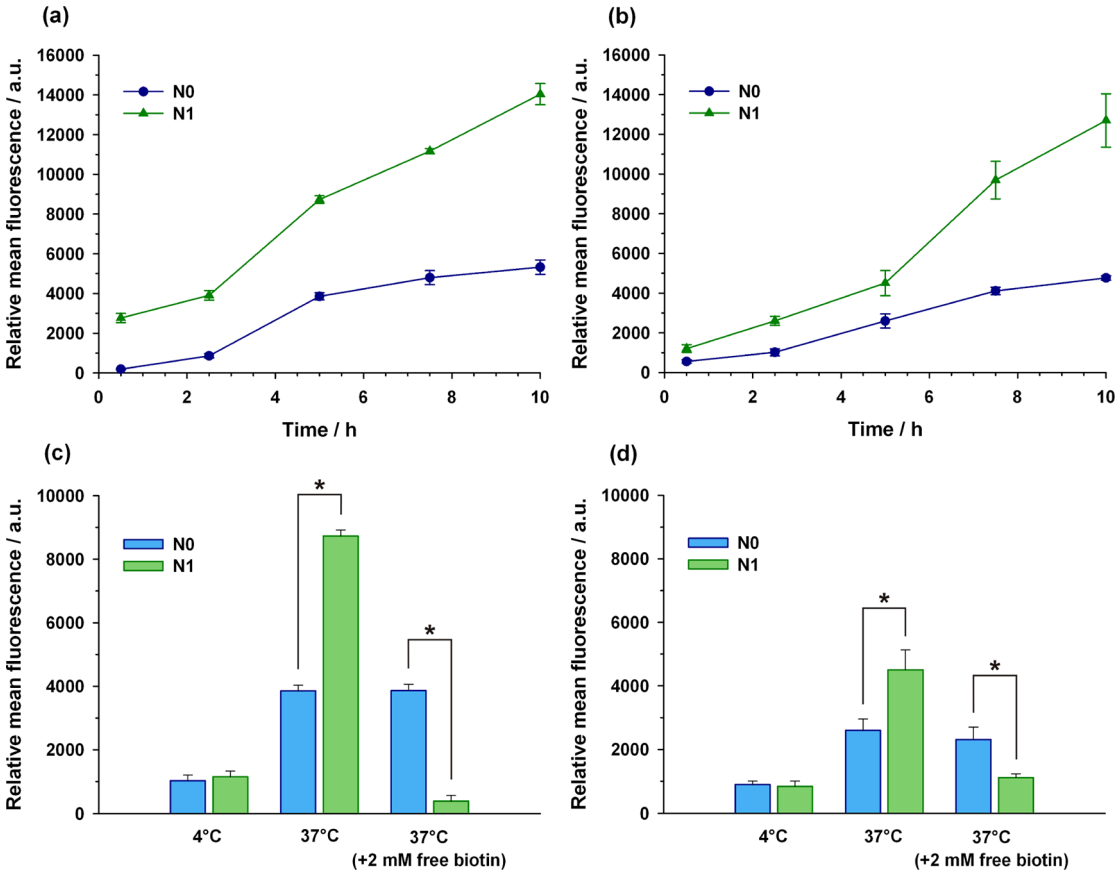

Figure 3. Kinetics of cellular uptake of nonfunctionalized (N0) and biotin-functionalized (N1) NPs in MCF7 (a) and M109 (b) cancer cells exposed to 100 $\mu g \cdot mL^{-1}$ of NPs. Internal rhodamine B fluorescence in cells after 5 h of MCF7 (c) or M109 (d) exposure to 100 $\mu g \cdot mL^{-1}$ of NPs at 4 and 37 °C in the presence or in the absence of 2 mM of free biotin. Statistical differences are expressed by an asterisk (*) ($p < 0.01$).

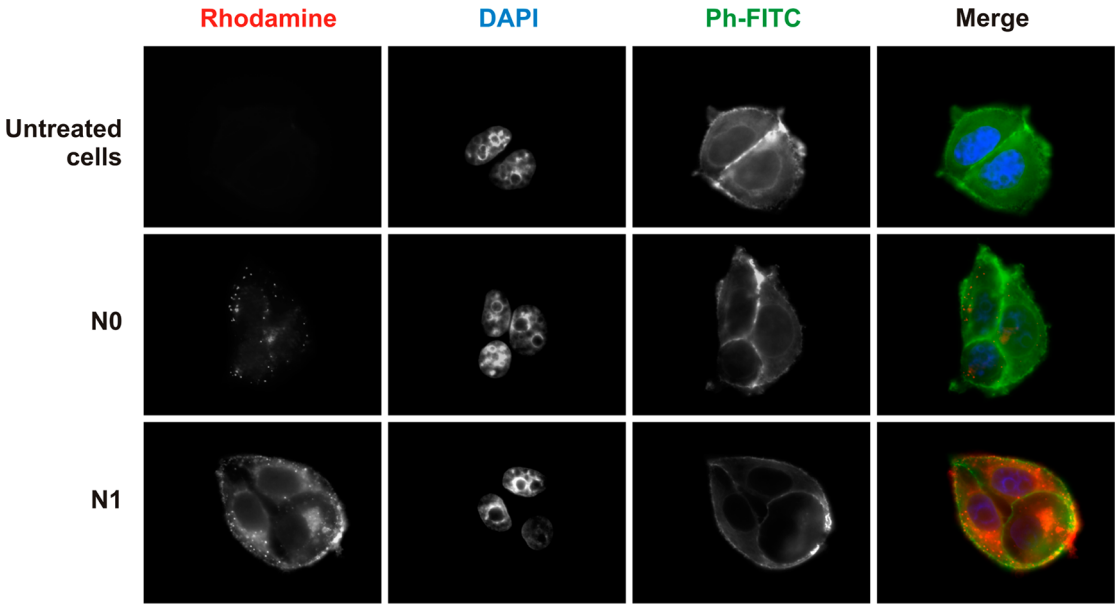

Figure 4. Internalization of rhodamine B-labeled NPs. Fluorescence microscopy images of MCF7 cells showing the cellular uptake of nonfunctionalized (N0) and biotin-functionalized (N1) NPs (red) after 5 h of incubation. The nuclei were stained with DAPI (blue), phalloidin−fluorescein isothiocyanate (Ph-FITC, green) was used to label F-actin, and the last column represents the overlay of all types of staining.

are encapsulated.[34] Not only this confirmed the formation of mixed NPs (*i.e.*, biotinylated and fluorescent nanocomposites) rather than two independent sets of NPs, but it also allowed to support an endocytic

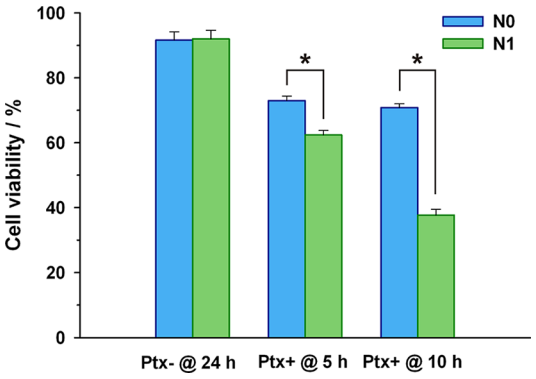

Figure 5. Cell viability of MCF7 cells after exposure to empty (Ptx-) and paclitaxel-loaded (Ptx+) NPs N0 and N1 at a Ptx concentration of 1.2 μM. Statistical differences are expressed by an asterisk (*) ($p < 0.01$).

mechanism as fluorescence was mainly localized into vesicles surrounding the nuclei.

Cytotoxicity against Cancer Cells. The biotin-functionalized (**N1**) nanoparticles were further tested *in vitro* for their therapeutic efficacy against MCF7 cancer cells using encapsulated paclitaxel (Ptx), one of the most important anticancer agents in clinical use. The reduction of cell viability caused by nanoparticles **N0** and **N1**, either empty (Ptx-) or loaded with paclitaxel (Ptx+) at a concentration of 1.2 μM (see the Experimental Section and Supporting Information, Figures S8,S9) is reported in Figure 5. Ptx-loaded, nonbiotinylated NPs **N0** led to a slight reduction of cell viability, but constant over time, comparatively to empty nanoparticles, probably due to some burst release of Ptx in the cell culture medium (the so-called burst effect). In contrast, biotin-labeled NPs **N1** loaded with Ptx conducted to a significantly higher cytotoxicity at 5 h incubation compared to their nonbiotinylated counterparts **N0**, which was even more pronounced at 10 h (<40% cell viability). It is worth mentioning that the half maximal inhibitory concentration (IC_{50}) was already reached at 10 h with 1.2 μM of Ptx, thus demonstrating the high anticancer activity of Ptx loaded into biotin-functionalized nanoparticles.

Selectivity of the Targeting. Because anticancer treatments usually lack cell specificity and do not discriminate healthy cells from cancerous ones, causing some severe adverse effects, we first performed uptake experiments using NPs **N0** and **N1** with noncancer human endothelial umbilical vein cells (HUVEC) not overexpressing biotin receptors (Supporting Information, Figures S10c,d). In this case, a poor uptake was obtained without any noticeable influence of the temperature or the addition of 2 mM of free biotin, showing the absence of targeting *via* the biotin-receptor-mediated pathway.

The high selectivity of the targeting was further consolidated by a coculture experiment in which healthy NIH/3T3 cells (stained in green) were cocultured with cancer MCF7 cells (unstained), and subsequently incubated with NPs **N1** (rhodamine B-labeled, red). The aim was to determine whether healthy cells can be saved from nanoparticle recognition and if a specific targeting toward cancer MCF7 cells can occur. Remarkably, after 2 h, biotin-functionalized, rhodamine-labeled NPs **N1** showed a strong internalization in MCF7 cells, whereas no internalization was noticeable in NIH/3T3 cells (Figure 6). This high targeting selectivity toward cancer cells was even observed up to 10 h incubation.

In summary, the presence of overexpressed biotin receptor at the surface of the human breast adenocarcinoma MCF7 and murine lung cancer M109 cell lines was used to demonstrate the efficient and highly selective targeting ability of our PACA nanoparticulate platform, using biotin as the cell-targeting moiety and rhodamine B as the fluorescent marker.

Targeting Aβ_{1-42} Monomers and Fibrils. *Interaction with Curcumin-Functionalized NPs.* Several studies have reported the functionalization of curcumin on various monomers or polymer templates by means of the CuAAC reaction.[42,43] So far for colloidal systems, only functionalization at the surface of liposomes has been achieved, leading to increased binding affinity toward Aβ_{1-42} monomer/fibrils.[44]

Prior to interaction studies, cell viability assays were performed by the MTT test in order to determine the cytotoxicity of curcumin-functionalized NPs **N2**–**N3** on hCMEC/D3 cells. This cell line has been validated as a unique immortalized *in vitro* model of human BBB and appeared relevant if AD therapy is envisioned. As depicted in Supporting Information, Figure S11, no statistical difference in NPs **N2**–**N3** cytotoxicity was observed up to a copolymer concentration of 50 $\mu g \cdot mL^{-1}$, which was comparable to the cytotoxicity of their nonfunctionalized counterparts **N0**.

The ability of these nanoconstructs to interact with the Aβ_{1-42} peptide was investigated by means of SPR experiments. To this purpose, the curcuminoid-functionalized NPs **N2** and **N3**, as well as the corresponding nonfunctionalized counterpart **N0**, used as a control, were made to flow over parallel channels of the same sensor chip immobilizing Aβ_{1-42} monomers or Aβ_{1-42} fibrils. Other parallel channels, naked or immobilizing BSA, were used as reference surfaces. As expected with NPs **N0** and **N2**-**N3**, no binding was detected onto the two reference surfaces (data not shown). However, a clear binding signal was observed for immobilized Aβ_{1-42}, in particular Aβ_{1-42} fibrils, with all types of NPs (Figure 7), including the nonfunctionalized ones **N0**, in good agreement with a preliminary study showing that PEGylated PACA NPs could interact to a certain extent with Aβ_{1-42} monomers.[45] Nevertheless, no increase of binding compared to **N0** was observed after NP functionalization with **Cur^{A}** (**N2**), for which the curcuminoid was attached to the PEG chain *via* an aromatic ring (Figure 7a,b). On the contrary for

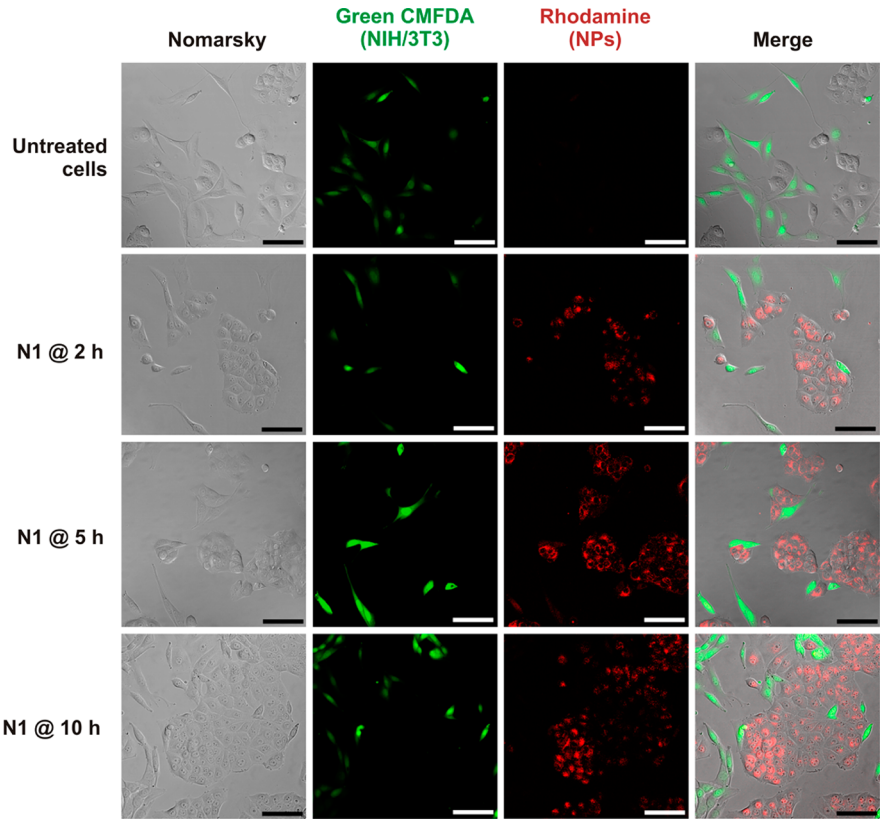

Figure 6. Nomarsky and confocal laser-scanning microscopy images of a coculture of NIH/3T3 (green) and MCF7 cells (unstained) after incubation with biotin-functionalized, rhodamine-labeled (N1) NPs (red) at 40 $\mu g \cdot mL^{-1}$ at different time intervals (2, 5, and 10 h). The NIH/3T3 cells were stained with Green CMFDA (green). Scale bars = 100 μm.

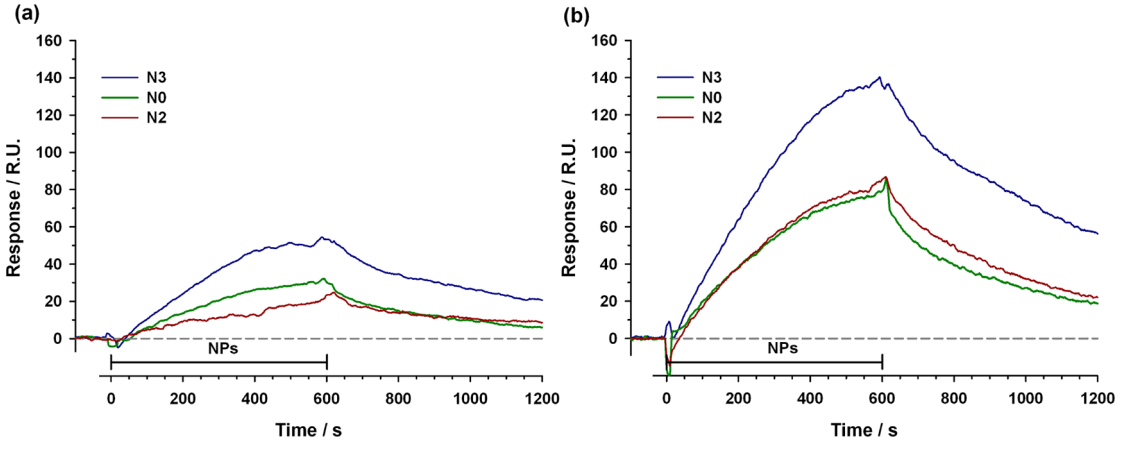

Figure 7. SPR sensorgrams (resonance units, RU, *versus* time) obtained by simultaneous injections of Cur^A-functionalized (N2), Cur^B-functionalized (N3), and nonfunctionalized (N0) NPs for 10 min (bars) over $A\beta_{1-42}$ monomers (a) or fibrils (b) immobilized on two parallel channels of the same sensor chip. The final concentration of the curcuminoid was 240 nM.

NPs **N3** displaying **Cur^B**, a marked increase of binding compared to **N0** was observed, indicating that the use of **Cur^B** as a ligand conferred additional binding properties to these NPs toward $A\beta_{1-42}$ monomers and the corresponding fibrils. The equilibrium dissociation constant (K_D) values of exposed **Cur^B** for $A\beta$ monomers and fibrils were in the submicromolar range, of about 0.8 and 0.3 μM, respectively.

The marked discrepancy concerning the binding ability of NPs **N2** and **N3** toward $A\beta_{1-42}$ monomers and fibrils was further explained by a difference of stability of the curcumin derivatives in aqueous solution. Nonmodified curcumin is indeed known to be highly unstable, undergoing rapid hydrolytic degradation in neutral or alkaline conditions.[46] A stability study was performed with **Cur^A** and **Cur^B** by means of ^{1}H NMR in PBS (pH 7.4) and revealed that **Cur^A** was totally degraded after only 15 min whereas **Cur^B** was still intact after 7 days incubation (Supporting Information, Figures S12). In the latter case, the formation of the

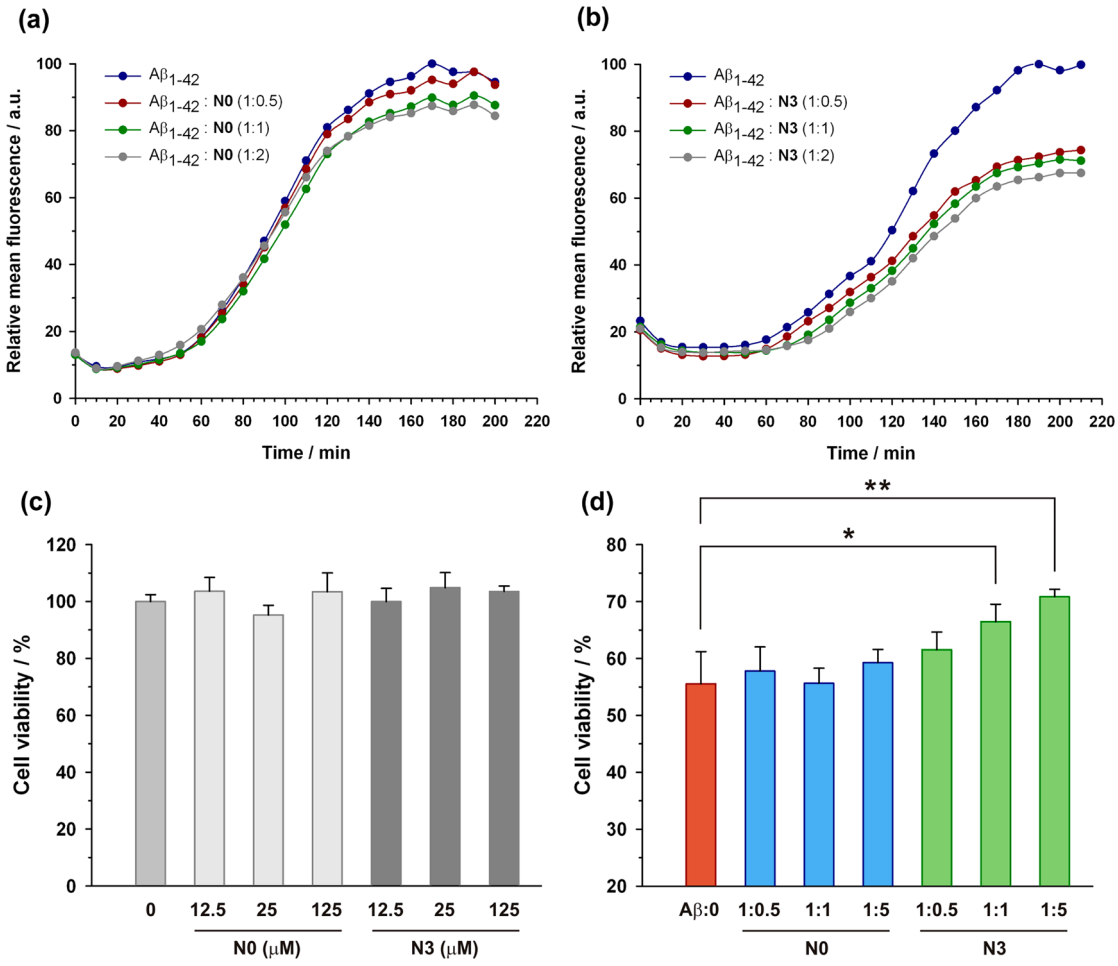

Figure 8. Effects of NPs on the aggregation of Aβ_{1-42} using the Thioflavin T binding assay (a and b). Aggregation kinetics of 25 μM Aβ_{1-42} alone or coincubated with increasing molar ratios (1:0.5; 1:1 and 1:2) of nonfunctionalized (N0) (a) or Cur^{B}-functionalized (N3) (b). NPs. Data are shown as mean (n = 3) from a representative experiment of three independent experiments. Effects of NPs on Aβ_{1-42} toxicity using an MTT viability assay (c and d). Differentiated SK-N-SH cells were treated for 48 h in the absence or in the presence of different concentrations of NPs N0 or N3 (12.5; 25 or 125 μM) to assess toxicity of the NPs (c); by differentiated SK-N-SH cells were treated for 48 h in the absence or presence of Aβ_{1-42} (25 μM) preaggregated in PBS for 24 h at 25 °C, alone or in combination with three different molar ratios (1:0.5; 1:1 and 1:5) of NPs N0 or N3 (d), to address interference of the NPs with Aβ toxicity. Cell viability was measured using a MTT assay and is depicted as a percentage of the untreated cells (control). The graph represents the mean ± SD (n = 4) from one experiment and results shown are representative for three independent experiments. Statistical differences are expressed by asterisks: (*) $p < 0.05$ and (**) $p < 0.01$.

pyrazole moiety avoids the presence of the chemically labile β-diketone group and, at the same time, locks the keto−enol tautomerism in an enol-type arrangement, crucial for Aβ binding effect.[44,47−49]

Since curcumin is known to inhibit Aβ_{1-42} aggregation, the effect of **Cur^{B}**-functionalized NPs on Aβ_{1-42} aggregation was analyzed by a Thioflavin T (ThT) binding assay. As shown in Figure 8a,b, **Cur^{B}**-functionalized NPs **N3** inhibited the aggregation of Aβ_{1-42} in a dose-dependent manner, while the nonfunctionalized NPs **N0** at the same concentrations only poorly affected the Aβ_{1-42} aggregation, highlighting the specific effect of the **Cur^{B}**-functionalization. Notably, the aggregation inhibition of Aβ_{1-42} by NPs **N3** was observed at a submolar ratio (1:0.5).

To investigate whether the interference of the **Cur^{B}**-functionalized NPs **N3** with the aggregation of Aβ_{1-42} could affect Aβ_{1-42} cytotoxicity, we performed an MTT assay on differentiated human neuroblastoma cells (SK-N-SH), which is a relevant model to study the targeting of Aβ neurotoxicity. Also in this model, no toxicity of NPs **N0** and **N3** was observed (Figure 8c). SK-N-SH cells were then treated with aggregated Aβ_{1-42} peptide in the absence or in the presence of increasing molar ratios of NPs **N0** or **N3** in order to address whether NPs could interfere with Aβ toxicity. In accordance with ThT data, the samples treated with NPs **N3** showed a concentration-dependent protective effect compared to the samples treated with Aβ_{1-42} alone, whereas control NPs (**N0**) did not significantly affect cell survival (Figure 8d). This indicated that intervention in aggregation by NPs did not create toxic Aβ species and even conducted to a noticeable toxicity rescue. In conclusion, it was clearly shown that

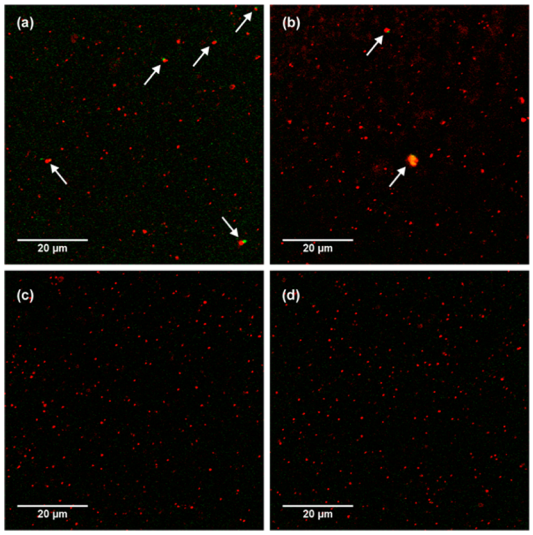

Figure 9. Confocal laser scanning microscopy images of nonfunctionalized (N0) and biotin-functionalized (N1) NP suspensions (20 μM) incubated with fluorescein-labeled streptavidin (FITC-SAv): N1, [FITC-SAv] = 0.2 μM (a); N1, [FITC-SAv] = 0.5 μM (b); N0, [FITC-SAv] = 0.2 μM (c); and N0, [FITC-SAv] = 0.5 μM (d).

Cur^B-functionalized NPs significantly inhibited both the aggregation and the toxicity of Aβ_{1-42} at low molar ratios.

Design of Anti-Aβ_{1-42}-functionalized Nanoparticles and Interaction with Aβ_{1-42}. Although **Cur^B**-functionalized NPs **N3** led to an increased interaction with Aβ_{1-42} monomer/fibrils by means of specific aromatic binding,[37] we decided to go a step further by designing a truly specific and even more efficient Aβ-binding nanocarrier. Thanks to the presence of biotin at the surface of NPs **N1**, previously employed for cancer cell targeting, we took advantage of the versatility of this nanoparticulate platform to decorate the NPs with a novel monoclonal anti-Aβ_{1-42} antibody (mAb) by means of the biotin/streptavidin (SAv) ligation strategy. The availability of the exposed biotin to SAv was confirmed by confocal laser scanning microscopy (CLSM) as shown in Figure 9. A fluorescein-tagged streptavidin (SAv-FITC) was incubated with either biotin-functionalized (**N1**) or nonfunctionalized (**N0**) NPs. Only in the case of **N1** were some NPs-SAv-FITC aggregates observed *via* the formation of clearly colocalized bigger size aggregates (note that the SAv-FITC concentration was chosen so as to be in the same range as the exposed biotin for **N1**). This result was further confirmed by SPR experiments showing strong binding of NPs **N1** to avidin-immobilized chip (Supporting Information, Figure S13), compared to nonfunctionalized NPs **N0** or **N1** flowed over noncoated chip (*i.e.*, ethanolamine surface). The amount of surface available biotin on NPs **N1** per gram of nanoparticle was quantified by the competitive avidin/HABA binding assay (see the Supporting Information) and gave 5360 nmol·g^{-1}. When compared to the theoretical value (*i.e.*, 29400 nmol·g^{-1}), the fraction of surface-available biotin is ~18%, which is consistent with literature data.[50]

A streptavidin-anti Aβ_{1-42} antibody conjugate was prepared (Supporting Information) and characterized by PAGE electrophoresis (Figure S14). Visualization under UV excitation (λ = 488 nm) revealed the presence of the conjugate characterized by a higher molecular weight when compared to native SAv-FITC, while a SAv-FITC/anti-Aβ_{1-42} mAb physical mixture did not show any coupling product. A suspension of NPs **N1** was then incubated with the SAv-FITC-anti-Aβ_{1-42} mAb conjugate followed by a centrifugation step that allowed anti-Aβ_{1-42} mAb-functionalized NPs **N4** to be isolated (D_z = 151 nm $\pm$ 24 nm) from unreacted species. A Bradford's assay revealed that 37% of the SAv-FITC-anti-Aβ_{1-42} mAb conjugate were bound to the surface of the NPs, whereas this amount was as low as 10% with nonfunctionalized NPs **N0** (*i.e.*, due to aspecific adsorption of Aβ_{1-42} mAb at the surface of **N0**). The MTT assay showed that NPs **N4** were not cytotoxic up to 50 μg·mL^{-1} (Figure S11).

The ability of NPs **N4** to specifically interact with Aβ_{1-42} was investigated by SPR experiments on monomeric or fibrillar peptide (Figure 10). As expected, a strong interaction was obtained with NPs **N4** (60 μM), whereas no or only a weak signal was observed under identical experimental conditions with either nonfunctionalized NPs **N0** or with a physical mixture of **N0** and anti-Aβ_{1-42} mAb, further purified from free mAb (data not shown). Moreover, NPs **N4** led to a dose−response behavior, allowing the equilibrium dissociation constants to be determined. The affinity of the mAb-functionalized NPs **N4** for the peptide was very high and exhibited K_D values in the picomolar range (monomers, K_D ~700 pM; fibrils, K_D ~300 pM). K_D values for the free mAb were about 150 and 240 pM for monomers and fibrils, respectively (data not shown). These data clearly indicated that the functionalization with the anti-Aβ_{1-42} mAb conferred to the corresponding NPs a remarkable ability to strongly bind the Aβ_{1-42} peptide (as monomer or as aggregated fibrils), and that the procedure used for NP functionalization only slightly altered the affinity for the peptide. It is worth noting that the affinity of the NPs **N4** for Aβ_{1-42} species was higher than any other colloidal systems reported so far.[44,48,49,51]

CONCLUSIONS

This study described the design of a new versatile and ligand-functionalized poly(alkyl cyanoacrylate) nanoparticulate platform, gathering together all crucial features required for targeting and drug delivery. Multifunctional NPs arising from this platform were successfully used to target two major pathologies, namely cancer and Alzheimer's disease, *via* their functionalization by appropriate biologically active ligands.

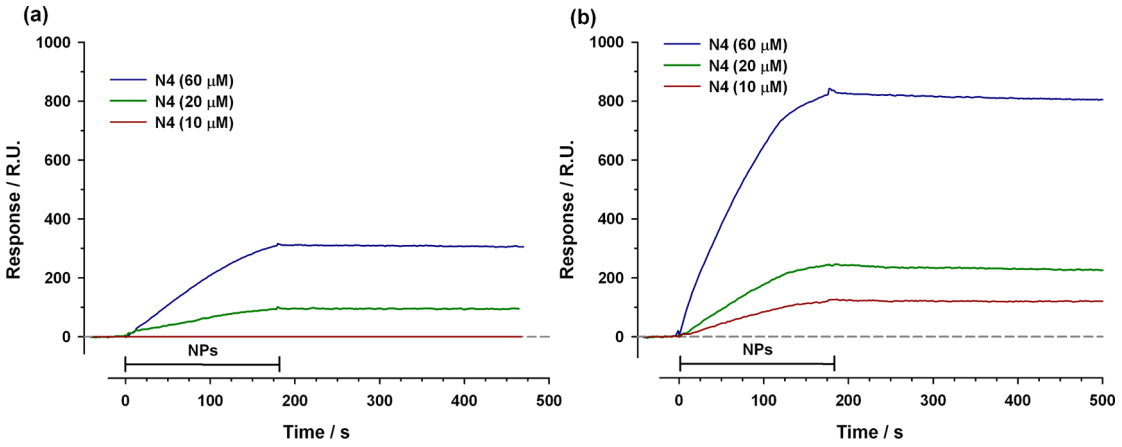

Figure 10. SPR sensorgrams (resonance units, RU, *versus* time) of anti-Aβ_{1-42} mAb-functionalized (N4) NPs at various concentrations (10, 20, 60 μM), flowed for 3 min (bars) onto a Aβ_{1-42} monomer (a) or Aβ_{1-42} fibrils (b) immobilized on the sensor chip.

These nanocarriers exhibited (i) a biodegradable core; (ii) stealth features due to a PEG outer shell; (iii) fluorescent properties provided by the covalent linkage of a fluorescent probe; and (iv) biologically active ligands displayed at their surface to achieve active targeting.

Regarding potential cancer therapy, biotin has been used as a ligand for specific recognition of different cancer cell lines, while letting noncancer cells or cancer cells with nonoverexpressed biotin receptors be unaffected, even in a healthy/cancer cells coculture environment. This strategy is now applicable to a variety of anticancer agents by simple encapsulation into the PACA polymeric matrix using the robust methodologies already developed before, and could have important clinical applications for cancer therapy. In this view, the encapsulation of paclitaxel, one of the most important anticancer agents in clinical use, has been achieved and led to a strong toxicity against cancer cells with biotin-functionalized NPs. Interestingly, because drug-loaded PACA NPs have been shown to overcome cancer MDR, it is expected that the biotin-functionalized PACA NPs described here may open a more specific avenue toward the treatment of solid tumors that are hard to treat by conventional chemotherapy.

In the field of AD, both curcumin derivatives as well as a specific anti-Aβ_{1-42} antibody were positioned at the surface of PACA NPs which exhibited strong affinity toward Aβ_{1-42} monomers and the corresponding fibrils. In the case of the anti-Aβ_{1-42} mAb, the biotin/streptavidin ligation strategy was employed, using biotin-functionalized NPs as the same colloidal system that served to target cancer cells. Dissociation rate constants in the picomolar range were obtained, which represent the highest values ever reported for colloidal systems so far. With curcumin functionalization, the resulting NPs offered a significant aggregation inhibition of Aβ_{1-42} together with a marked toxicity rescue, both at low molar ratios.

The proposed synthetic pathway is therefore very flexible and adaptable for applications to a broad range of pathologies, simply by adjusting the surface functionalization of the nanocarriers by means of suitable ligands.

EXPERIMENTAL SECTION

Synthesis Methods. Synthesis of Curcumin^A-poly(ethylene glycol) (**Cur^A**PEG), Curcumin^B-poly(ethylene glycol) (**Cur^B**PEG), Curcumin^A-poly(ethylene glycol) cyanoacetate (**Cur^A**PEGCA), Curcumin^B-poly(ethylene glycol) cyanoacetate (**Cur^B**PEGCA), biotin-poly(ethylene glycol) (**VB7**PEG), biotin-poly(ethylene glycol) cyanoacetate (**VB7**PEGCA), anti-Aβ_{1-42} antibody and Anti-Aβ_{1-42} antibody-fluorescein labeled streptavidin bioconjugate (mAb-SAv) are detailed in the Supporting Information. HDCA, MePEGCA, P(MePEGCA-*co*-HDCA) copolymer **C0** ($M_{n,SEC}$ = 2430 g·mol^{-1}, M_w/M_n = 1.27) and the fluorescent rhodamine-B-tagged P(MePEGCA-*co*-RCA-*co*-HDCA) copolymer **C1** ($M_{n,SEC}$ = 2270 g·mol^{-1}, M_w/M_n = 1.30) were prepared according to previously published procedures.[34,52]

General Copolymerization Procedure for the Preparation of Biotin-Functionalized P(MePEGCA-*co*-VB7PEGCA-*co*-HDCA) Copolymers C2. In a 25 mL round-bottom flask containing HDCA (170 mg, 550 μmol, 40 equiv), MePEGCA (229 mg, 110 μmol, 8 equiv), and **VB7**PEGCA (65 mg, 27.5 μmol, 2 equiv or 20 mol % in the initial PEG cyanoacetate mixture) monomers, CH_2Cl_2 (2.84 mL) and EtOH (1.42 mL) under magnetic stirring, were sequentially introduced formaldehyde (345 μL, 4.63 mmol) and pyrrolidine (14.5 μL, 176 μmol). The mixture was allowed to stir for 24 h at room temperature and was then concentrated under reduced pressure. The residue was taken into CH_2Cl_2 and washed multiple times with water. The resulting organic layer was dried over $MgSO_4$, filtered, concentrated under reduced pressure and dried under vacuum to give a brown, waxy solid. Quantification of **VB7**PEGCA in the copolymer was estimated by ^{1}H NMR that confirmed the presence of 20 mol % **VB7**PEGCA monomer insertion (when compared to the overall PEGCA content in the polymerization feed). $M_{n,SEC}$ = 2160 g·mol-1, M_w/M_n = 1.34.

General Copolymerization Procedure for the Preparation of Poly-[Hexadecyl Cyanoacrylate-*co*-Cur^{A}PEGcyanoacrylate-*co*-methoxypoly(ethylene glycol) Cyanoacrylate] (P(HDCA-*co*-Cur^{A}PEGCA-*co*-MePEGCA), C3) and Poly-[hexadecyl cyanoacrylate-*co*-Cur^{B}PEGcyanoacrylate-*co*-methoxypoly(ethylene glycol) Cyanoacrylate] (P(HDCA-*co*-Cur^{B}PEGCA-*co*-MePEGCA), C4) Copolymers. In a 25 mL round-bottom flask containing MePEGCA (258 mg, 124 μmol, 9 equiv), HDCA (170 mg, 550 μmol, 40 equiv), **Cur^{A}**PEGCA (34 mg, 13.8 μmol, 10 mol % in the initial PEG cyanoacetate mixture or 1 equiv) or **Cur^{B}**PEGCA (35 mg, 13.8 μmol, 1 equiv) monomers, EtOH (1.42 mL) and CH_2Cl_2 (2.84 mL) under magnetic stirring, were sequentially introduced formaldehyde (345 μL, 4.6 mmol) and pyrrolidine (14.5 μL, 176 μmol). The mixture was allowed to stir for 24 h at room temperature and was then concentrated under reduced pressure. The residue was taken into CH_2Cl_2 and washed multiple times with water. The resulting organic layer was dried over $MgSO_4$, filtered, concentrated under reduced pressure and dried under vacuum to give the resulting copolymers. Quantification of **Cur^{A}**PEGCA or **Cur^{B}**PEGCA in the copolymer was estimated by ^{1}H NMR that confirmed the presence of about 10 mol % curcumin-functionalized PEGCA (when compared to the overall PEGCA content in the polymerization feed).

Nanoparticle Preparation. Fluorescent NPs **N0** were prepared by the nanoprecipitation technique using a 50/50 blend of P(MePEGCA-*co*-HDCA) (**C0**) and P(MePEGCA-*co*-RCA-*co*-HDCA) (**C1**) copolymers. Fluorescent and functionalized **N1**-**N3** NPs were prepared by the nanoprecipitation technique using a 50/50 blend of P(MePEGCA-*co*-RCA-*co*-HDCA) (**C1**) and P-(MePEGCA-*co*-**VB7**PEGCA-*co*-HDCA) (**C2**), P(MePEGCA-*co*-**Cur^{A}**-PEGCA-*co*-HDCA) (**C3**), or P(MePEGCA-*co*-**Cur^{B}**PEGCA-*co*-HDCA) (**C4**) copolymers, respectively (see Table 1 for details). Briefly, 5 mg of each copolymer was dissolved in acetone (2 mL), and the copolymer solution was added dropwise to an aqueous solution 0.5% (w/v) of Pluronic F-68 (4 mL) under vigorous mechanical stirring. Acetone was then evaporated under reduced pressure, and NPs were purified by ultracentrifugation (150 000*g* for **N0**, **N2**−**N3**, and 82 000*g* for **N1**, 1 h, 4 °C, Beckman Coulter, Inc.). The supernatant was discarded and the pellet was resuspended in the appropriate volume of deionized water to yield a 2.5 mg·mL^{-1} nanoparticle suspension.

Paclitaxel-loaded NPs **N0** and **N1** were prepared by the emulsion/solvent evaporation technique using the same copolymer blends as previously described for nonbiotinylated (**C0**/**C1**) or biotinylated (**C0**/**C2**) NPs. Briefly, 5 mg of each copolymer was dissolved in 1 mL of 1 mg·mL^{-1} organic solution of paclitaxel (chloroform/ethanol 90/10 v/v). To this organic phase was added 4 mL of an aqueous solution of PVA (0.25% w/w) presaturated with 1% chloroform. The resulting emulsion was vortexed two times for 1 min at 2400 rpm and ultrasonicated on ice for 3 min at 150 V using a sonicating device (Ultrasons Annemasse, France). The solvent was then removed under reduced pressure to yield a stable suspension of NPs. NPs were purified by filtration on 1 μm glass fiber membrane (Acrodisc, Pall) slide. Paclitaxel-loaded NPs were further purified by centrifugation for 20 min at 17 000*g* and 20 °C. After 24 h, a second centrifugation step was performed. NPs were stored at 20 °C until use. To assess the Ptx concentration, NPs were radiolabeled by entrapment of ^{3}H-paclitaxel. A 100 μL aliquot of radioactive drug dissolved in ethanol (10 μCi) was added to 900 μL of chloroform solution in which the blend of polymers and the nonradiolabeled paclitaxel have been previously dissolved. NPs were then prepared according to the same experimental procedure as described before. After the second centrifugation step, 500 μL of NPs were placed in the scintillation counting vials and 10 mL of Ultima Gold scintillant was added. The mixture was vortexed vigorously for 1 min. Then, the radioactivity present in the samples was measured (n = 3) using a liquid scintillation counter (Beckman, LS 6000TA; Beckman Coulter). In both cases, drug encapsulation efficiency was 1.1%. For *in vitro* cytotoxicity experiments, Ptx-loaded NPs were tested at a concentration of 1.2 μM_{Ptx}.

Cell Culture. hCMEC/D3 cells were grown in EBM-2 basal medium (Lonza, Belgium) supplemented with fetal bovine serum 5% (FBS, Lonza, Belgium), hydrocortisone 1.4 μM, basic fibroblast growth factor 1 ng·mL^{-1}, pen-strep 1%, and HEPES 10 mM. Murine lung carcinoma cell lines M109, human breast cancer cell lines MCF7, human endothelial umbilical vein cells (HUVEC), murine leukemia cells (L1210), and embryonic murine fibroblast (NIH/3T3) were obtained from the American Type Culture Collection and maintained as recommended. Briefly, M109 and L1210 cells were maintained in RPMI 1640 medium (Lonza, Belgium). MCF7, SK-N-SH, HUVEC, NIH/3T3 cells were grown in Dulbecco's modified Eagle's medium (DMEM, Lonza, Belgium) supplemented with 50 U·mL^{-1} penicillin, 50 U·mL^{-1} streptomycin, and 10% heat-inactivated FBS. Cells were maintained in a humid atmosphere at 37 °C with 5% CO_2.

Coculture. NIH/3T3 fibroblasts (5×10^4) were plated onto microscopic glass slides and incubated for 18 h at 37 °C and 5% CO_2 in cell culture medium. To visualize and distinguish between NIH/3T3 fibroblasts and MCF7 cells in coculture, NIH/3T3 cells were stained with 5 μM CellTracker green 5-chloromethylfluorescein diacetate (CMFDA, Life Technology, Molecular Probes) according to the manufacturer's protocol. After staining, cells were left to rest for 2 h at 37 °C and 5% CO_2 in cell culture medium, followed by addition of unstained MCF7 cells (15×10^4). The seeding ratio between MCF7 and NIH/3T3 cells was 1:3 due to the faster doubling time of the latter. After 12 h, the coculture was incubated with NPs (**N1**) diluted in fresh cell culture medium at 40 μg·mL^{-1}. At different time points (2, 5, and 10 h) cells were washed with prewarmed culture medium before imaging.

Cytotoxicity Studies. The cytotoxicity of NPs **N0**−**N4** was investigated by MTT [3-(4,5-dimethylthiazol-2-yl)-2,5-diphenyl tetrazolium bromide] viability test on hCMEC/D3 human brain endothelial cell line. Briefly, cells were grown on 10 cm diameter plates in EBM-2 basal medium supplemented with fetal bovine serum 5%, hydrocortisone 1.4 μM, basic fibroblast growth factor 1 ng·mL^{-1}, penicillin/streptomycin solution 1%, ascorbic acid 5 μg·mL^{-1}, Chemically Defined Lipid Concentrate (1/100), and HEPES 10 mM. Polystyrene 96 wells plates were used and cells were seeded in each well (75 000 cells·mL^{-1}) with the medium previously described. After a 2 days growth, an aqueous suspension of NPs was incubated at five different concentrations: 10, 20, 30, 50, and 100 μg·mL^{-1}. After 48 h of incubation at 37 °C in 5% CO_2, the MTT reagent (at a final concentration of 0.05% in Dulbecco's PBS, D-PBS) was added and 3 h later, the percentage of living cells was evaluated with a 96 wells plate absorbance reader at 570 nm. Cells treated with the same volume of water were used as negative controls.

A MTT viability test was also performed with **N0** and **N1** NPs on MCF7 and M109 cell lines. Briefly, 10000 MCF7 or 5000 M109 cells per well were incubated in 200 μL of medium containing 10% FBS in 96-well plates for 24 h. The cells were then exposed to a series of concentrations of **N1** NPs for 24 h. After drug exposition, the medium was removed and 100 μL of MTT solution (0.5 mg·mL^{-1} in DMEM containing 10% FBS) was added to each well. The plates were incubated for 2 h at 37 °C, and 100 μL of 20% SDS solution was then added to each well for 24 h at 37 °C. Absorbance was measured at 570 nm using a plate reader (Perkin-Elmer). All experiments were set up in quadruplicate to determine means and SDs. We examined the antiproliferative effect of the studied NPs on the growth of a murine lung carcinoma and human breast cancer cell lines (M109 and MCF7). For further studies, the noncytotoxic concentration of NPs (*i.e.*, 100 μg·mL^{-1}) was used.

For toxicity of NPs **N0** and **N3**, SK-N-SH cells were plated in 96-well plates at a density of 20×10^3 cells per well and differentiated for 5 days in medium supplemented with 10 μM retinoic acid (Sigma). HFIP treated Aβ_{1-42} was dissolved in DMSO and subsequently diluted in PBS. A 25 μM aliquot of Aβ_{1-42} containing different concentrations of NPs (12.5, 25, or 125 μM) was then incubated for 24 h at 25 °C. This mixture was diluted 25 times into DMEM without phenol red and added in quadruplicate to differentiated SK-N-SH. After 48 h of incubation at 37 °C in 5% CO_2, the MTT reagent (at a final concentration of 0.05% in D-PBS) was incubated for 2 h, and subsequently the insoluble formazan salt generated by the viable cells was solubilized in DMSO. The number of viable cells was directly quantified by measuring the absorbance at

570 nm. Viability was expressed as a percentage of untreated cells.

Cell-Internalization of Biotin-Labeled Nanoparticles. In this study we used MCF7 human breast adenocarcinoma and M109 murine lung carcinoma cell lines with increased expression of biotin receptors.[32,35] MCF7 cancer cells were cultured on a coverslip in a culture dish for 24 h to achieve approximately 40% confluence. Cells were then incubated with NPs **N0** and **N1** at a concentration of 100 $\mu g \cdot mL^{-1}$ (37 °C) for 5 h. After treatment, the cells were washed with D-PBS, fixed in 3% paraformaldehyde (PFA), stained with phalloidin−fluorescein isothiocyanate (Ph-FITC, 200 μM) and DAPI (40 μM) (Invitrogen), washed with D-PBS five times, and imaged using a fluorescence microscope (Leica) with a ×63 oil-immersion objective. The following wavelengths were used: excitation at 488 nm and detection through a 515 nm filter for FITC, and excitation at 488 nm and detection through a long-pass 560 nm filter for rhodamine B.

To quantitatively measure the internalization of biotin-functionalized NPs **N1**, MCF7 or M109 cells (2×10^5) were cultured on 6-well plates for 24 h to achieve 60−80% confluence. NPs **N1** and control **N0** NPs were then added at the noncytotoxic concentration of 100 $\mu g \cdot mL^{-1}$ to each well. After incubation for determined times (0.5, 2.5, 5, 7.5, and 10 h), the cells were collected for measurement of rhodamine B fluorescence. The fluorescence from individual cells was examined using a flow cytometer C6 (Accuri Cytometers Ltd., UK). For fluorescence detection of NPs, excitation was carried out with the 488-nm line of an argon laser, and emission fluorescence between 560 and 606 nm was measured. For all experiments in which the intracellular rhodamine B was quantified using a flow cytometer, 10000 cells were measured from each sample. For low temperature experiments, the cells were incubated in the cold room at 4 °C for 5 h. For competition experiments, cells were preincubated at 37 °C for 1 h in the presence of free biotin at the concentration of 2 mM. All experiments were set up in triplicate to determine means and SDs.

Interaction Experiments between Curcumin-Functionalized NPs (N2 and N3) and Aβ_{1-42} Monomers/Fibrils. Aβ_{1-42} monomers or fibrils were obtained from the in-house depsi peptide as previously described.[53] They were immobilized in parallel-flow channels of a GLC sensor chip (Biorad) using amine-coupling chemistry. Briefly, after sensor surface activation, the peptide solutions (10 μM in acetate buffer pH 4.0) were injected for 5 min at a flow rate of 30 $\mu L \cdot min^{-1}$, and the remaining activated groups were blocked with ethanolamine, pH 8.0. The final immobilization levels were about 2000 Resonance Units (1 RU = 1 pg protein$\cdot mm^{-2}$) for both Aβ_{1-42} monomers and fibrils. Bovine serum albumin (BSA) was also immobilized, in a parallel flow channel as a reference protein and another reference surface was prepared in parallel using the same immobilization procedure but without addition of the peptide (naked surface). Preliminary injections were performed in order to check the binding features of the immobilized species. The anti-Aβ antibody 6E10 (Covance) was injected and, as expected, bound to both Aβ fibrils and monomers (not shown) whereas Congo-Red, a dye specifically recognizing β-sheet-containing species, only bound to Aβ fibrils but not monomers (not shown). The suspensions of curcumin-functionalized P(MePEGCA-*co*-PHDCA) NPs **N2** and **N3** were diluted and injected onto immobilized Aβ species or the reference surfaces. All the injections were carried out for 5 min at a flow rate of 30 $\mu L \cdot min^{-1}$ at 30 °C in PBST (PBS + 0.005% Tween20, pH 7.4).

Interaction Experiments between Biotin-Functionalized NPs (N1) and Avidin. Avidin (which is a protein having the same activity as streptavidin) was immobilized on a channel of a CM5 sensor chip (Biacore, GE Healthcare) using amine-coupling chemistry. Briefly, after sensor surface activation by EDC/NHS, the avidin solution (50 $\mu g \cdot mL^{-1}$ in acetate buffer pH 5.0) was injected for 7 min at a flow rate of 10 $\mu L \cdot min^{-1}$, and the remaining activated groups were blocked with ethanolamine, pH 8.0. The final immobilization levels were about 8500 Resonance Units (1 RU = 1 pg protein$\cdot mm^{-2}$), that is, 8.5 ng$\cdot mm^{-2}$. Another parallel channel, on which ethanolamine blocked the surface (empty surface), using the same immobilization procedure but without addition of avidin (immobilization level about 23 RU), was used as a reference channel. The 10% biotin-functionalized **N1** NP suspension was diluted at a 1 $mg \cdot mL^{-1}$ final concentration and flowed onto both channels for 10 min. The same experiments were performed with rhodamine B-tagged nonfunctionalized NPs **N0** as negative controls.

The interaction between streptavidin and biotin-functionalized NPs was also demonstrated using fluorescein-tagged streptavidin (SAv-FITC) and rhodamine B-labeled 10% biotin-functionalized **N1** NPs. Increasing volumes of a 20 mM phosphate buffer saline solution of SAv-FITC (5 $mg \cdot mL^{-1}$, 94 μM) were incubated for 15 min with a 20 μM suspension of rhodamine B-labeled 10% biotin-functionalized **N1** NP suspension to reach final SAv-FITC concentrations of 0.2, 0.5, 1, 2, and 20 μM. A 10 μL deposit of this final incubation sample on glass coverslips was visualized by confocal laser scanning microscopy (CLSM) under both fluorescence channels. The same experiments were performed with rhodamine B-tagged nonfunctionalized **N0** NPs as negative controls.

Preparation of Anti-Aβ_{1-42} Antibody Functionalized NPs (N4). To 34 μL of a suspension of **N1** NPs was added 1 mL of the anti-Aβ_{1-42}-streptavidin conjugate solution (see the Supporting Information for details). The resulting suspension was gently shaken for 30 min before purification by ultracentrifugation at 150 000*g* for 1 h at 4 °C. The amount of anti-Aβ_{1-42}-mAb-streptavidin conjugate linked to the NPs was determined by Bradford's assay. The anti-Aβ_{1-42}-mAb functionalized **N4** NPs were used without further purification.

Interaction Experiments between Anti-Aβ_{1-42}-Functionalized NPs (N4) and Aβ_{1-42} Monomers/Fibrils. Aβ_{1-42} monomeric or fibrillar preparations were obtained from the commercial peptide (Sigma) as previously described, and the presence of monomers or fibrils was checked by atomic force microscopy (AFM) (data not shown).[48] SensiQ semiautomatic apparatus with two parallel flow channels was employed (ICX Technologies). A COOH5 sensor chip (ICX Technologies) was installed in the system, and monomers were immobilized using amine-coupling chemistry on one channel, while the other one was used as reference surface. In the same way, a second COOH5 sensor chip was used for the immobilization of fibrils.

Briefly, after sensor surface activation, the peptide solution (10 μM in acetate buffer pH 4.0) was flowed for 5 min at a rate of 30 $\mu L \cdot min^{-1}$, and the remaining activated groups were blocked with ethanolamine, pH 8.0. The final immobilization levels were about 4000 Resonance Units (1 RU = 1 pg protein$\cdot mm^{-2}$). The reference surface was prepared in parallel using the same immobilization procedure but without the addition of the peptide (naked surface). Preliminary injections with the anti-Aβ antibody 6E10 (Covance) were performed and, as expected, it bound to both Aβ fibrils and monomers. The suspensions of NPs **N4** were diluted and injected. The same experiments were performed with nonfunctionalized NPs **N0** as well as with a physical mixture of **N0** and anti-Aβ_{1-42} mAb, (purified from the free mAb) as negative controls. All the injections were carried out for 3 min at a flow rate of 30 $\mu L \cdot min^{-1}$ at 30 °C in PBST (PBS + 0.005% Tween20, pH 7.4).

Conflict of Interest: The authors declare no competing financial interest.

Acknowledgment. The authors warmly thank Dr. Claire Boulogne for the TEM analysis, Valérie Nicolas (Plateforme Imagerie Cellulaire, IFR 141) for her help with the CLSM, and Dario Carradori for his help on the HABA assay. This work has used the facilities and the expertises of the (Electron Microscopy Platform) Cell biology unit of the Imagif platform (Centre de Recherche de Gif). The research leading to these results has received funding from the European Community's Seventh Framework Programme (FP7/2007-2013) under agreement no. 212043. The CNRS and the French Ministry of Research are also warmly acknowledged for financial support.

Supporting Information Available: Detailed experimental section [materials, synthesis of **Cur^A**PEG, synthesis of **Cur^B**PEG, synthesis of **Cur^A**PEGCA, synthesis of **Cur^B**PEGCA, synthesis of **VB7**PEG, synthesis of **VB7**PEGCA, synthesis of anti-Aβ_{1-42}

antibody, synthesis of anti-Aβ_{1-42} antibody-fluorescein-labeled streptavidin bioconjugate, nuclear magnetic resonance (NMR) spectroscopy, size exclusion chromatography (SEC), dynamic light scattering (DLS), transmission electron microscopy (TEM), surface plasmon resonance (SPR), avidin/HABA competitive binding assay, thioflavin T assay, confocal laser scanning microscopy (CLSM), NMR evaluation of compound Cur^{A} and Cur^{B} chemical stability, Anti-Aβ_{1-42} antibody-SAv complex quantification at the surface of rhodamine B labeled P(MePEGCA-*co*-**VB7**PEGCA-*co*-HDCA) NPs, DLS and TEM data for NPs **N0**−**N3**], supporting Figures **S1**−**S14**. This material is available free of charge *via* the Internet at http://pubs.acs.org.

REFERENCES AND NOTES

1. Brigger, I.; Dubernet, C.; Couvreur, P. Nanoparticles in Cancer Therapy and Diagnosis. *Adv. Drug Delivery Rev.* **2002**, *54*, 631–651.
2. Brambilla, D.; Le Droumaguet, B.; Nicolas, J.; Hashemi, S. H.; Wu, L.-P.; Moghimi, S. M.; Couvreur, P.; Andrieux, K. Nanotechnologies for Alzheimer's Disease: Therapy, Diagnosis and Safety Issues. *Nanomedicine: NBM* **2011**, *7*, 521–540.
3. Farokhzad, O. C.; Langer, R. Impact of Nanotechnology on Drug Delivery. *ACS Nano* **2009**, *3*, 16–20.
4. Sanhai, W. R.; Sakamoto, J. H.; Canady, R.; Ferrari, M. Seven Challenges for Nanomedicine. *Nat. Nanotechnol.* **2008**, *3*, 242–244.
5. Erb, S. E. Nanotechnology in Drug Delivery. *Drug Delivery Syst.* **2009**, *24*, 63–70.
6. Riehemann, K.; Schneider, S. W.; Luger, T. A.; Godin, B.; Ferrari, M.; Fuchs, H. Nanomedicine-Challenge and Perspectives. *Angew. Chem., Int. Ed.* **2009**, *48*, 872–897.
7. Arias, J. L.; Reddy, L. H.; Othman, M.; Gillet, B.; Desmaële, D.; Zouhiri, F.; Dosio, F.; Gref, R.; Couvreur, P. Squalene Based Nanocomposites: A New Platform for the Design of Multifunctional Pharmaceutical Theragnostics. *ACS Nano* **2011**, *5*, 1513–1521.
8. Hans, M. L.; Lowman, A. M. Biodegradable Nanoparticles for Drug Delivery and Targeting. *Curr. Opin. Solid State Mater. Sci.* **2002**, *6*, 319–327.
9. Panyam, J.; Labhasetwar, V. Biodegradable Nanoparticles for Drug and Gene Delivery to Cells and Tissue. *Adv. Drug Delivery Rev.* **2003**, *55*, 329–347.
10. Brannon-Peppas, L. Recent Advances on the Use of Biodegradable Microparticles and Nanoparticles in Controlled Drug Delivery. *Int. J. Pharm.* **1995**, *116*, 1–9.
11. Sinha, R.; Kim, G. J.; Nie, S.; Shin, D. M. Nanotechnology in Cancer Therapeutics: Bioconjugated Nanoparticles for Drug Delivery. *Mol. Cancer Ther.* **2006**, *5*, 1909–1917.
12. Soppimath, K. S.; Aminabhavi, T. M.; Kulkarni, A. R.; Rudzinski, W. E. Biodegradable Polymeric Nanoparticles as Drug Delivery Devices. *J. Controlled Release* **2001**, *70*, 1–20.
13. Cabral, H.; Nishiyama, N.; Kataoka, K. Supramolecular Nanodevices: From Design Validation to Theranostic Nanomedicine. *Acc. Chem. Res.* **2011**, *44*, 999–1008.
14. Couvreur, P.; Vauthier, C. Nanotechnology: Intelligent Design to Treat Complex Disease. *Pharm. Res.* **2006**, *23*, 1417–1450.
15. Sukhorukov, G. B.; Rogach, A. L.; Zebli, B.; Liedl, T.; Skirtach, A. G.; Köhler, K.; Antipov, A. A.; Gaponik, N.; Susha, A. S.; Winterhalter, M.; *et al.* Nanoengineered Polymer Capsules: Tools for Detection, Controlled Delivery, and Site-Specific Manipulation. *Small* **2005**, *1*, 194–200.
16. Zhang, F.; Lees, E.; Amin, F.; Rivera_Gil, P.; Yang, F.; Mulvaney, P.; Parak, W. J. Polymer-Coated Nanoparticles: A Universal Tool for Biolabelling Experiments. *Small* **2011**, *7*, 3113–3127.
17. Sperling, R. A.; Rivera Gil, P.; Zhang, F.; Zanella, M.; Parak, W. J. Biological Applications of Gold Nanoparticles. *Chem. Soc. Rev.* **2008**, *37*, 1896–1908.
18. Laurent, S.; Forge, D.; Port, M.; Roch, A.; Robic, C.; Vander Elst, L.; Muller, R. N. Magnetic Iron Oxide Nanoparticles: Synthesis, Stabilization, Vectorization, Physicochemical Characterizations, and Biological Applications. *Chem. Rev.* **2008**, *108*, 2064–2110.
19. Kelkar, S. S.; Reineke, T. M. Theranostics: Combining Imaging and Therapy. *Bioconjugate Chem.* **2011**, *22*, 1879–1903.
20. Barraud, L.; Merle, P.; Soma, E.; Lefrançois, L.; Guerret, S.; Chevallier, M.; Dubernet, C.; Couvreur, P.; Trépo, C.; Vitvitski, L. Increase of Doxorubicin Sensitivity by Doxorubicin-Loading into Nanoparticles for Hepatocellular Carcinoma Cells *in Vitro* and *in Vivo*. *J. Hepatol.* **2005**, *42*, 736–743.
21. Fattal, E.; Youssef, M.; Couvreur, P.; Andremont, A. Treatment of Experimental Salmonellosis in Mice with Ampicillin-Bound Nanoparticles. *Antimicrob. Agents Chemother.* **1989**, *33*, 1540–1543.
22. Calvo, P.; Gouritin, B.; Villarroya, H.; Eclancher, F.; Giannavola, C.; Klein, C.; Andreux, J. P.; Couvreur, P. Quantification and Localization of Pegylated Polycyanoacrylate Nanoparticles in Brain and Spinal Cord During Experimental Allergic Encephalomyelitis in the Rat. *Eur. J. Neurosci.* **2002**, *15*, 1317–1326.
23. Reddy, L. H.; Couvreur, P. Nanotechnology for Therapy and Imaging of Liver Diseases. *J. Hepatol.* **2011**, *55*, 1461–1466.
24. Peracchia, M. T.; Desmaële, D.; Couvreur, P.; d'Angelo, J. Synthesis of a Novel Poly(MePEG cyanoacrylate-*co*-alkyl cyanoacrylate) Amphiphilic Copolymer for Nanoparticle Technology. *Macromolecules* **1997**, *30*, 846–851.
25. Calvo, P.; Gouritin, B.; Chacun, H.; Desmaele, D.; D'Angelo, J.; Noel, J. P.; Georgin, D.; Fattal, E.; Andreux, J. P.; Couvreur, P. Long-Circulating Pegylated Polycyanoacrylate Nanoparticles as New Drug Carrier for Brain Delivery. *Pharm. Res.* **2001**, *18*, 1157–1166.
26. Brigger, I.; Morizet, J.; Aubert, G.; Chacun, H.; Terrier-Lacombe, M. J.; Couvreur, P.; Vassal, G. Poly(ethylene glycol)-Coated Hexadecylcyanoacrylate Nanospheres Display a Combined Effect for Brain Tumor Targeting. *J. Pharmacol. Exp. Ther.* **2002**, *303*, 928–936.
27. Nicolas, J.; Couvreur, P. Synthesis of Poly(alkyl cyanoacrylate)-Based Colloidal Nanomedicines. *Wiley Interdiscip. Rev. Nanomed. Nanobiotechnol.* **2009**, *1*, 111–127.
28. Müller, R. H.; Lherm, C.; Herbort, J.; Couvreur, P. *In Vitro* Model for the Degradation of Alkylcyanoacrylate Nanoparticles. *Biomaterials* **1990**, *11*, 590–595.
29. Low, P. S.; Henne, W. A.; Doorneweerd, D. D. Discovery and Development of Folic-Acid-Based Receptor Targeting for Imaging and Therapy of Cancer and Inflammatory Diseases. *Acc. Chem. Res.* **2008**, *41*, 120–129.
30. Lu, Y.; Low, P. S. Folate-Mediated Delivery of Macromolecular Anticancer Therapeutic Agents. *Adv. Drug Delivery Rev.* **2002**, *54*, 675–693.
31. Lu, Y.; Sega, E.; Leamon, C. P.; Low, P. S. Folate Receptor-Targeted Immunotherapy of Cancer: Mechanism and Therapeutic Potential. *Adv. Drug Delivery Rev.* **2004**, *56*, 1161–1176.
32. Lee, E. S.; Na, K.; Bae, Y. H. Super pH-Sensitive Multifunctional Polymeric Micelle. *Nano Lett.* **2005**, *5*, 325–329.
33. Kolb, H. C.; Finn, M. G.; Sharpless, K. B. Click Chemistry: Diverse Chemical Function from a Few Good Reactions. *Angew. Chem., Int. Ed.* **2001**, *40*, 2004–2021.
34. Brambilla, D.; Nicolas, J.; Le Droumaguet, B.; Andrieux, K.; Marsaud, V.; Couraud, P.-O.; Couvreur, P. Design of Fluorescently Tagged Poly(alkyl cyanoacrylate) Nanoparticles for Human Brain Endothelial Cell Imaging. *Chem. Commun.* **2010**, *46*, 2602–2604.
35. Russell-Jones, G.; McTavish, K.; McEwan, J.; Rice, J.; Nowotnik, D. Vitamin-Mediated Targeting as a Potential Mechanism to Increase Drug Uptake by Tumours. *J. Inorg. Biochem.* **2004**, *98*, 1625–1633.
36. Kelloff, G. J.; Crowell, J. A.; Hawk, E. T.; Steele, V. E.; Lubet, R. A.; Boone, C. W.; Covey, J. M.; Doody, L. A.; Omenn, G. S.; Greenwald, P.; *et al.* Strategy and Planning for Chemopreventive Drug Development: Clinical Development Plans II. *J. Cell. Biochem.* **1996**, *63*, 54–71.
37. Porat, Y.; Abramowitz, A.; Gazit, E. Inhibition of Amyloid Fibril Formation by Polyphenols: Structural Similarity and Aromatic Interactions as a Common Inhibition Mechanism. *Chem. Biol. Drug Des.* **2006**, *67*, 27–37.

38. Ono, K.; Hasegawa, K.; Naiki, H.; Yamada, M. Curcumin Has Potent Anti-amyloidogenic Effects for Alzheimer's B-Amyloid Fibrils *in Vitro*. *J. Neurosci. Res.* **2004**, *75*, 742–750.
39. Yang, F.; Lim, G. P.; Begum, A. N.; Ubeda, O. J.; Simmons, M. R.; Ambegaokar, S. S.; Chen, P. P.; Kayed, R.; Glabe, C. G.; Frautschy, S. A.; *et al*. Curcumin Inhibits Formation of Amyloid β Oligomers and Fibrils, Binds Plaques, and Reduces Amyloid *in Vivo*. *J. Biol. Chem.* **2005**, *280*, 5892–5901.
40. Reinke, A. A.; Gestwicki, J. E. Structure−Activity Relationships of Amyloid Beta-Aggregation Inhibitors Based on Curcumin: Influence of Linker Length and Flexibility. *Chem. Biol. Drug Des.* **2007**, *70*, 206–215.
41. Thielbeer, F.; Donaldson, K.; Bradley, M. Zeta Potential Mediated Reaction Monitoring on Nano and Microparticles. *Bioconjugate Chem.* **2011**, *22*, 144–150.
42. Ouberai, M.; Dumy, P.; Chierici, S.; Garcia, J. Synthesis and Biological Evaluation of Clicked Curcumin and Clicked Klvffa Conjugates as Inhibitors of B-Amyloid Fibril Formation. *Bioconjugate Chem.* **2009**, *20*, 2123–2132.
43. Shi, W.; Dolai, S.; Rizk, S.; Hussain, A.; Tariq, H.; Averick, S.; L'Amoreaux, W.; El Idrissi, A.; Banerjee, P.; Raja, K. Synthesis of Monofunctional Curcumin Derivatives, Clicked Curcumin Dimer, and a Pamam Dendrimer Curcumin Conjugate for Therapeutic Applications. *Org. Lett.* **2007**, *9*, 5461–5464.
44. Mourtas, S.; Canovi, M.; Zona, C.; Aurilia, D.; Niarakis, A.; La Ferla, B.; Salmona, M.; Nicotra, F.; Gobbi, M.; Antimisiaris, S. G. Curcumin-Decorated Nanoliposomes with Very High Affinity for Amyloid-B1−42 Peptide. *Biomaterials* **2011**, *32*, 1635–1645.
45. Brambilla, D.; Verpillot, R.; Taverna, M.; De Kimpe, L.; Le Droumaguet, B.; Nicolas, J.; Mantegazza, F.; Canovi, M.; Gobbi, M.; Salmona, M.; *et al*. Capillary Electrophoresis with Laser-Induced Fluorescence Detection (Ce-Lif) as a New Protocol to Monitor Interaction between Nanoparticles and the Amyloid-B Peptide. *Anal. Chem.* **2010**, *82*, 10083–10089.
46. Wang, Y.-J.; Pan, M.-H.; Cheng, A.-L.; Lin, L.-I.; Ho, Y.-S.; Hsieh, C.-Y.; Lin, J.-K. Stability of Curcumin in Buffer Solutions and Characterization of Its Degradation Products. *J. Pharm. Biomed. Anal.* **1997**, *15*, 1867–1876.
47. Airoldi, C.; Zona, C.; Sironi, E.; Colombo, L.; Messa, M.; Aurilia, D.; Gregori, M.; Masserini, M.; Salmona, M.; Nicotra, F.; *et al* . Curcumin Derivatives as New Ligands of Aβ Peptides. *J. Biotechnol.* **2011**, *156*, 317–324.
48. Gobbi, M.; Re, F.; Canovi, M.; Beeg, M.; Gregori, M.; Sesana, S.; Sonnino, S.; Brogioli, D.; Musicanti, C.; Gasco, P.; *et al* Lipid-Based Nanoparticles with High Binding Affinity for Amyloid-B1−42 Peptide. *Biomaterials* **2010**, *31*, 6519–6529.
49. Canovi, M.; Markoutsa, E.; Lazar, A. N.; Pampalakis, G.; Clemente, C.; Re, F.; Sesana, S.; Masserini, M.; Salmona, M.; Duyckaerts, C.; *et al*. The Binding Affinity of Anti-Aβ1−42 mab-Decorated Nanoliposomes to Aβ1−42 peptides *in Vitro* and to Amyloid Deposits in Postmortem Tissue. *Biomaterials* **2011**, *32*, 5489–5497.
50. Qi, K.; Ma, Q.; Remsen, E. E.; Clark, C. G., Jr.; Wooley, K. L. Determination of the Bioavailability of Biotin Conjugated onto Shell Crosslinked Nanoparticles. *J. Am. Chem. Soc.* **2004**, *126*, 6599–6607.
51. Brambilla, D.; Verpillot, R.; Le Droumaguet, B.; Nicolas, J.; Taverna, M.; Kóňa, J.; Lettiero, B.; Hashemi, S. H.; De Kimpe, L.; Canovi, M.; *et al*. Pegylated Nanoparticles Bind to and Alter Amyloid-Beta Peptide Conformation: Toward Engineering of Functional Nanomedicines for Alzheimer's Disease. *ACS Nano* **2012**, 10.1021/nn300489k.
52. Nicolas, J.; Bensaid, F.; Desmaele, D.; Grogna, M.; Detrembleur, C.; Andrieux, K.; Couvreur, P. Synthesis of Highly Functionalized Poly(alkyl cyanoacrylate) Nanoparticles by Means of Click Chemistry. *Macromolecules* **2008**, *41*, 8418–8428.
53. Beeg, M.; Stravalaci, M.; Bastone, A.; Salmona, M.; Gobbi, M. A Modified Protocol to Prepare Seed-Free Starting Solutions of Amyloid-B (Aβ)1−40 and Aβ1−42 from the Corresponding Depsipeptides. *Anal. Biochem.* **2011**, *411*, 297–299.